New Construction Methodology-Efficiency Improvements and Greenhouse Emissions Reduction for Combined Heat and Power (CHP) Reservoir Systems

J. Prakash Arul Jose[1]
[1]Department of Civil Engineering, Research Scholar,Bharath University, Chennai,India

Prof. Dr. P. Rajesh Prasanna [2]
[2]Professor, Department of Civil Engineering, Anna University Regional Center, Thiruchirappali-620 024.,India

Fleming Prakash[3]
[3]Department of Civil Engineering, PSG College of Technology, Coimbatore, India

1. INTRODUCTION

Simultaneous power generation and geosequestration make CO_2 a very attractive choice for geothermal power plants. As such, carbon-dioxide-based engineered geothermal systems (CO_2-EGS) have been previously proposed as an alternative to water-based EGS systems [1]. Additionally, [2] investigated the effects of CO_2 -rich phase compositions on the production flow rate and the heat extraction from the reservoir. What is yet to be reported in the literature is a detailed numerical simulation of a water-CO_2 mixture filling a reservoir. Simple thermodynamic analysis of a reservoir shows that more heat can be extracted (compared to a water saturated reservoir) mainly because a CO_2 -water mixture is more buoyant than pure water. Increasing penetration of distributed generation (DG) resources to the low voltage (LV) grids, such as Photovoltics, CHP micro-turbines, small wind turbines areas and possibly fuel cells, alters the traditional operating principle of the grids [3-5]. A particularly promising aspect, related to the proliferation of small-scale decentralized generations (μ sources), is the possibility for parts of the network comprising sufficient generating resources to operate in isolation from the main grid, in a deliberate and controlled way. These are called micro grids and the study and development of technology to permit their efficient operation has started with a great momentum [6,7].

Enhanced Geothermal Systems, also known as Engineered Geothermal Systems or Hot Dry Rock (HDR) systems, differ from the traditional hydrothermal systems in that the target reservoir typically consists of low permeability and low porosity rock with low fluid content and limited hydraulic connectivity between production and injection wells [8,9]. Hydraulic stimulation is required to enhance the permeability of the reservoir in order to create sufficient connectivity for water or perhaps CO_2 as heat transfer fluid. By recirculating fluid through the reservoir, the thermal energy stored in the hot rock mass gets extracted. Proper reservoir management using a “heat farming” strategy can ensure the renewability of the system on societal timescales [10-13]. Convective fluid plumes may play a role in enhancing heat flows from the mantle to geothermal reservoirs and within the reservoirs themselves. Additionally, convection within a geothermal reservoir may enhance the productive life-time of geothermal reservoir systems by enhancing heat supply from underlying strata and by ensuring a more even distribution of thermal energy throughout the reservoir, that is, by off-setting localized cooling along major flow paths [14-16].

As micro grid is able to supply its loads locally, it reduces the amount of power transfer from remote generation via transmission and distribution circuits. Hence, it will reduce system losses. This also leads to the reduction of total energy produced by central power plants. Thus, it will also reduce Pollutants (CO_2, NO_x, SO_2 and other particulate matter) from these plants.

2. MATERIALS AND METHODS

We anticipate this finding to have implications for the study of natural geothermal reservoirs, where the role of dissolved gas exsolution on heat transfer enhancement remains unquantified. Additionally, these findings may be of potential interest with regard to CO_2 injection into geothermal reservoirs, as it may lead to improved productivity through the mechanisms elucidated in this work. The magnitude of this effect on the thermal productivity of geothermal power plants is difficult at this stage to quantify and probably not meaningful to speculate on due to the limitation of assessing only single-phase flow behaviors within the reservoir.

2.1. Modeling. The reservoir is modeled as a bottom-heated square box with adiabatic lateral boundaries and a cold top wall as Figure 1 shows. The cold and hot temperatures are varied from 335 to 435 K and 425 to 525 K, respectively, in a way that the hot-cold temperature difference remains at 90 K for each case. For constant properties, and of course with the same reservoir size, porosity, and permeability, one would expect the results to be the same as long as the temperature difference is not altered. It will, however, be shown in the forthcoming sections that this is not the case in our problem as properties significantly vary with both temperature and pressure. The reservoir porosity is fixed at 0.05 and the permeability-length product is kept constant at $10^{-11} m^3$ similar

with no through-flow [17]. The reservoir pressure is varied from 20 to 60 MPa (equivalent to the hydrostatic pressure of approximately 2 to 6 km of water) to cover a wide range of practical applications for geothermal development.

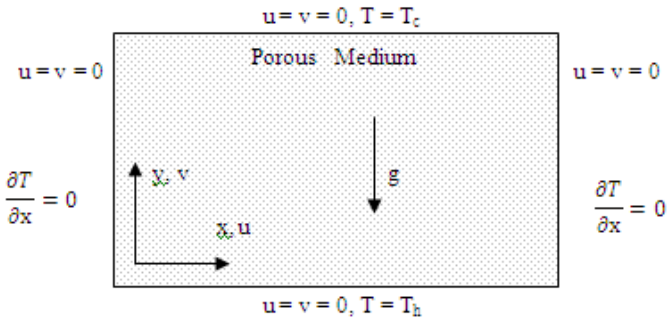

FIGURE 1: Schematic view of the computational domain.

2.2. Numerical Details. Grid independence was verified by running the software on different combination of grid sizes. It was observed that the results changed less than 2% when a 100 × 100 mesh system is used instead of a finer mesh with 200 × 200 grid points. Results are also verified for constant property free convection of water in a porous cavity, that is, the Darcy-Benard problem. It was noted that the correlation between Nusselt *number* (Nu) and Rayleigh number (Ra) Nu = Ra/40 best fits out numerical data, as Figure 2 shows.

2.3. Results and Discussions. In what follows we focus on free convection heat and fluid flow of a water-CO2 mixture in a porous cavity. We use Nu and maximum flow rate as our metrics to evaluate the strength of convective flow patterns. Nu is the total heat transfer divided by that of pure conduction through the same cavity (no convective flow patterns). As such, any Nu value in excess of unity shows some degree of convection. Obviously, higher Nu values mark stronger convective cells. The flow rate reported here is the one induced by free convection only, that is, without a well-head

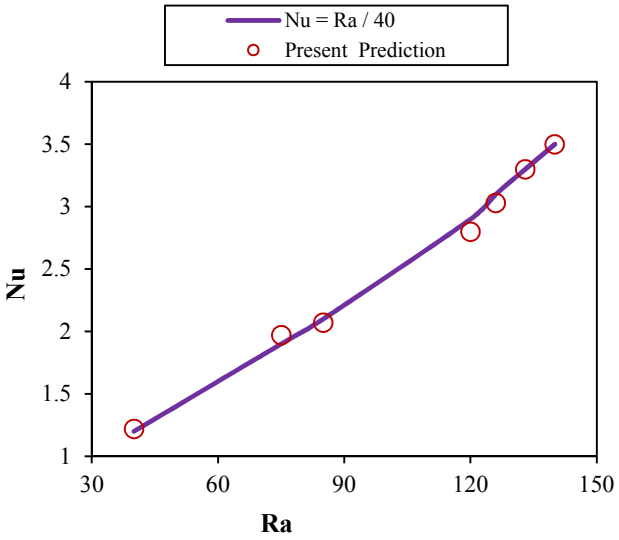

FIGURE 2: Validation of present CFD results against existing correlation for pure water.

pump or any other suction/injection mechanisms. We systematically change the CO_2 mass fraction from zero (pure water) to unity (pure CO_2) over a range of reservoir pressure and temperature in a way that the hot-cold temperature difference remains the same. For a constant property subcritical fluid flow, one would expect that, with the same temperature difference and, hence, the same Rayleigh number (Ra), the overall heat transfer and fluid flow will not alter. However, as CO_2 is supercritical within the range of conditions of underground reservoir systems, that is not the case for mixtures of CO2 and H2O, as demonstrated by Figure 3. This figure shows Nu versus CO_2 mass fraction at 20 MPa with the same hot-cold temperature difference but with different hot and cold temperatures as denoted on the plots. As seen, the heat transfer increases with CO2 mass fraction for any given *T*h and *Tc* combination. Furthermore, moving from pure water to pure CO, the increase in heat transfer is significant; about one order of magnitude is the minimal heat transfer augmentation. More interestingly, however, is the fact that Nu is the highest with the lowest *Tc* (and obviously lowest *T*h to maintain the same ΔT of 90 K) mainly because the lower temperatures are closer to those of pseudocritical conditions where Ra is expected to reach a maximum value [18,19]. This is obviously in favour of low temperature geothermal reservoirs which may not be productive when pure water is the working fluid.

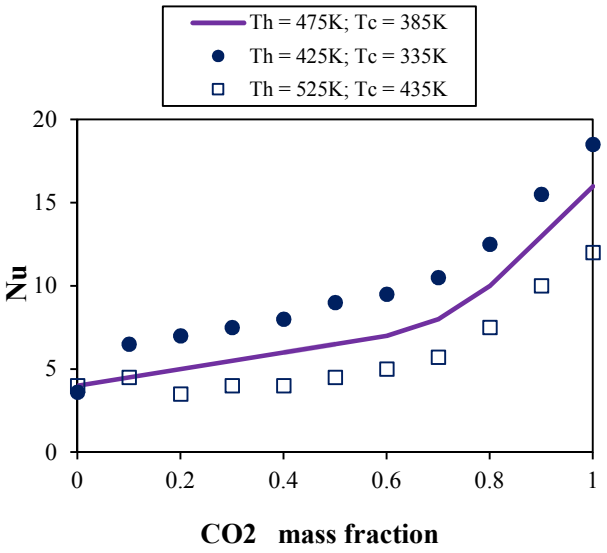

FIGURE 3: Nusselt number versus CO_2 mass fraction for different T_h and T_c combinations with ΔT = 90K.

Figures 4(a)–4(c) are presented to demonstrate Nu versus CO_2 mass fraction for different reservoir pressures and hotcold temperature combinations. Nu increases with mass fraction for a fixed pressure and hot-cold temperature combination. Comparing the relationship between any of Figures 4(a)–4(c) for a fixed pressure will result in conclusions similar to what were drawn based on close examination of Figure 3. That is, heat transfer increases for temperatures close to pseudocritical conditions. Moreover, based on plots in the same chart, increasing the pressure leads to lower heat transfer rates for a fixed CO_2 mass fraction and temperature. This could be explained as the obvious decrease in compressibility and

increase in the fluid density with higher pressures, with a fixed fluid temperature, which will lead to lower thermal expansion coefficients. As a result, at the same temperature, either of the two fluids will be less buoyant at higher pressures when compared to lower ones, so will be the mixture in the absence of any phase transitions. The convective flow rates also reflect a dependence on compressibility, as demonstrated by Figure 5.

The dimensionless flow rate (normalized stream function on the vertical axis) is obtained by normalizing the actual flow rate with appropriate scales for velocity, area, and density:

$$\varepsilon = \frac{m}{(\rho u A)} \qquad (1)$$

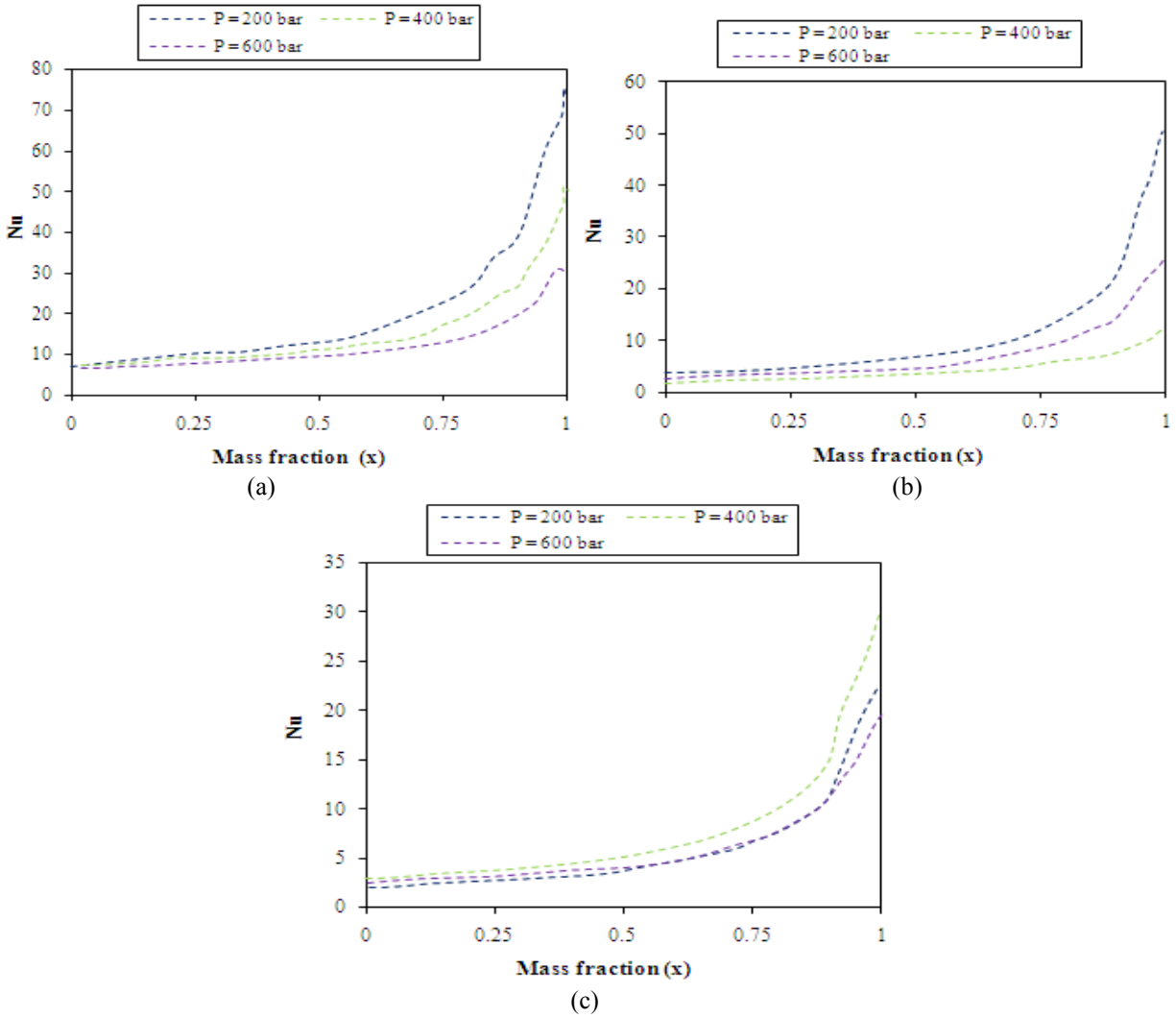

FIGURE 4 : Nusselt number versus CO_2 mass fraction for different reservoir pressures and temperature combinations : (a) T_h = 425K; T_c = 335K, (b) T_h = 475K; T_c = 385K, and (c) T_h = 525K; T_c = 435K.

Mathematically, it means that we used the group $\rho A u$ to non-dimensionalize the flow rate. It needs to be mentioned that the choice of these parameters is optional but we tried to use constant values for density and length to make it easy for the reader to generate estimates, based on our calculation, for expected flow rates through a given reservoir. Moreover, what we are more interested in is the trend of the flow rate plot against the mass fraction than the actual flow rate values.

In doing so, the (constant) density of water at atmospheric condition is used where the unit area is used defined as the length of the cavity multiplied by unity (1 m). The flow velocity, for single-phase constant property case, is assumed to be linearly proportional to the product of the thermal diffusivity and Ra1/2 and inverse linearly proportional to the cavity length; for example

$$u \sim \frac{\alpha}{H} \sqrt{Ra.} \qquad (2)$$

The flow rate is given by

$$m = \rho H u \sim \rho \alpha \sqrt{\text{Ra}}. \qquad (3)$$

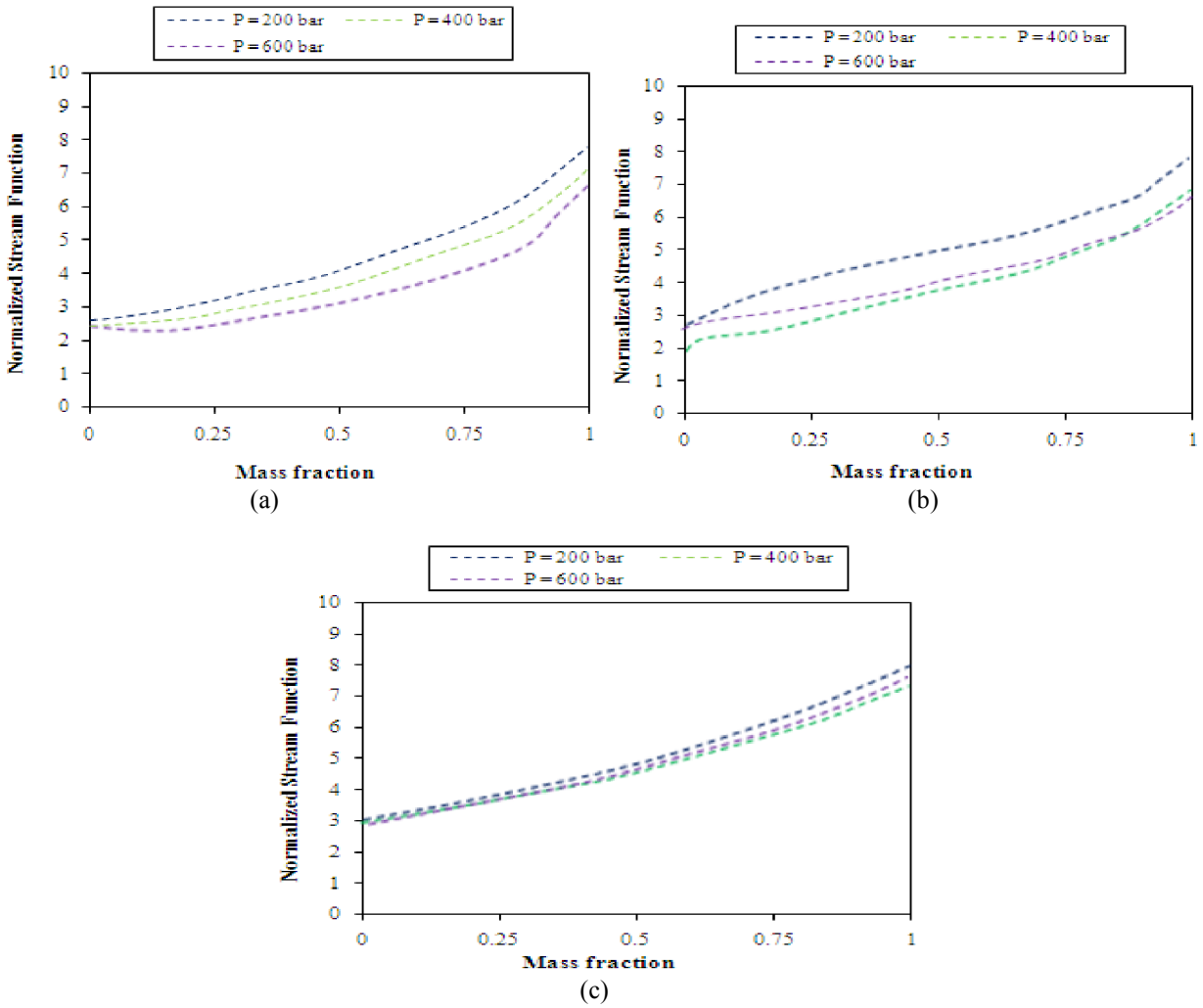

FIGURE 5: Dimensionless mass flow rate versus CO_2 mass fraction for different pressures and temperature combinations; (a) $T_h = 425K$; $T_c = 335K$, (b) $T_h = 475K$; $T_c = 385K$, and (c) $T_h = 525K$; $T_c = 435K$.

The product of thermal diffusivity and density is independent. This flow rate here is the buoyancy-induced flow rate due to changes in fluid density. The buoyancy-induced flow leads to an upward movement of hot fluid toward the top wall, where it is cooled and then displaced by other rising hot fluid. Results of mass flow rate normalized and presented in Figure 5 for different mass fractions, pressure, and temperature combinations. Similar to Nu plots, one notes that the mass flow rate is sensitive not only to the temperature difference but also to the actual wall temperature values. Furthermore, higher CO_2 mass fraction leads to higher flow rates. It can be noted, moving from Figures 5(a) to 5(c), that flow rates are less sensitive to pressure as *T*h is increased. With a fixed *T*h and Tc , one notes different trends in flow rate when pressure changes. Depending on the temperature values, an increase in pressure can either increase (Figure 5(a)) or decrease the flow rate (Figure 5(b)).

This work is an initial analysis of the role of CO_2 enhancement of convective heat transfer within geothermal reservoirs. It deliberately assesses the behavior of a single-phase mixture of the two components. Further work is necessary to extend this to account for multiple phases. There are three particular qualitative effects through which multiphase flow is expected to alter the results presented here. 1) Transient ex solution of dissolved CO_2 as bubbles within the two-phase region should lead to local enhancement of convective flow around the bubble due to its upwards buoyancy-driven motion. One expectation of this would be an increase in the gradient of convective heat flux with mass fraction (i.e., $d\xi/dx$) at the bubble line, where CO_2 begins to ex solve from the H_2O phase.

(2) Relative permeability within the two-phase region would act to reduce enhancement of flows, as the reservoir permeability to the minor phase within a two-phase flow is typically substantially reduced.

(3) Under steady- state conditions, there would be an expectation of phase separation into two horizontal phases based on relative density, that is, an upper CO_2 -rich phase and a lower H_2O-rich phase. The upper phase would experience significantly enhanced convective heat transfer rates, as it would have internal heat transfer characteristics similar to the right sides of Figures 4 and 5. Additionally, the heat transfer would be further enhanced by the temperature dependent solubility of H_2O in the CO_2 -rich phase, leading to additional H_2O evaporating into the CO_2 phase at the boundary between

the two phases and condensing at the upper surface of the reservoir. The H_2O-rich phase would experience the converse effect, depressing the rate of heat transfer, although CO solubility in H_2O is far less dependent on temperature than that of H_2O in CO_2 [20].

These expected qualitative behaviors require further analysis accounting for multiphase flow behavior to determine their relative contribution to overall convective heat flow enhancement. However, the sum of these changes is not expected to reverse the overall trend demonstrated here, of increased convective heat flux as CO_2 is added to the reservoir system. Considering that the results presented here indicate that CO_2 may enhance flow rates by up to a factor of 2.67, we conclude that this is a potentially important mode of heat transport within geothermal reservoirs and warrants further study. We anticipate the next steps to be consideration of the additional flow behaviors when multiple phases are present.

3. Benchmark Network Used for Analysis using Micro Grids

Distributed generation (DG) operation can improve the voltage profile in the micro grid nodes especially at the feeder where µ sources are installed. Therefore the installation of DG sources seems to be a solution in improving the voltage profile within a micro grid during times of low voltages (peak loads).

Bench mark network described in references [21,22] is used for analysis. Single line diagram with all buses marked is shown at the end of the paper (Figure 17). One feeder network includes 7 buses (buses 1-7) represent the residential loads. Industrial load (bus 8) represents the second feeder. The remaining buses (buses 9-16) feed commercial loads and represent the third feeder. Impedance of the network lines, data for µ sources used and renewable power time-series Used [output KW/Installed KW] are given in Tables 1-3 respectively [23].

The units have been calculated in power base of 100 KVA and voltage base 400V. Bus 0 represents the main grid (distribution network). Micro turbine is located at bus 7, fuel cell is located at bus 6, and PV_3 is located at bus 5 while wind turbine and PV_{2-5} are connected to bus 4.

3.1. Daily Load Curves for Single and Multiple Feeders Networks. Aggregate daily load curves for single feeder (residential loads) and three feeders (residential, industrial and com-mercial loads) are shown in Figure 6.

TABLE 1: Line data for micro grid.

Sending Bus	Receiving Bus	R (p.u.)	X (p.u.)
0	1	0.0025	0.01
1	2	0.0001	0.0001
2	3	0.0125	0.00375
3	4	0.0125	0.00375
4	5	0.0125	0.00375
5	6	0.0125	0.00375
3	7	0.021875	0.004375
1	8	0.033125	0.00875
1	9	0.0075	0.005
9	10	0.015	0.010625
10	11	0.02125	0.005625
11	12	0.02125	0.005625
9	13	0.010625	0.005625
13	14	0.010625	0.005625
10	15	0.023125	0.00625
15	16	0.023125	0.00625

TABLE 2: Data of the used µ sources.

Unit ID	Unit Name	Minimum capacity (KW)	Minimum capacity (KW)
1	Micro turbine	2	30
2	Fuel Cell	1	30
3	Wind	0.1	15
4	PV_1	0.05	3
5	PV_2	0.05	2.5
6	PV_3	0.05	2.5
7	PV_4	0.05	2.5
8	PV_5	0.05	2.5

TABLE 3: Renewable power time-series (Output KW/Installed KW).

Hour	Wind Power	PV- Time series
1	0.364	0
2	0.267	0
3	0.267	0
4	0.234	0
5	0.312	0
6	0.329	0
7	0.476	0.002
8	0.477	0.008
9	0.424	0.035
10	0.381	0.1
11	0.459	0.23
12	0.39	0.233
13	0.494	0.318
14	0.355	0.433
15	0.433	0.37
16	0.321	0.403
17	0.329	0.33
18	0.303	0.238
19	0.364	0.133
20	0.373	0.043
21	0.26	0.003
22	0.338	0
23	0.312	0
24	0.346	0

3.2. Voltage Enhancement and Power Losses Saving Evaluation with Using Micro Grid. Load flow program [24] is used to calculate the voltages at all nodes of the micro grid. Results are shown in Figures 7-12. The power factor is 0.85 lagging for residential and commercial consumers and 0.9 for the industrial ones. All calculations have been made at p.u of base V_{base}= 400 V and S_{base} = 100 KVA. The network data are presented in Sections 2 and 3. It has also been assumed that in the µ sources the power electronic interface has been adjusted to give or absorb zero reactive power at all base buses except fuel cell and micro turbine buses. At all time, we assume that the micro turbine and fuel cell operated at 84% of their maximum capacity (25 KW), and the renewable sources outputs powers as listed in Table 3.

The dashed lines represent results without µ sources while the solid lines represent results With using µ sources.

From the above results the following points can be raised:

i) With using µ sources, in the two studied cases (single feeder and three feeder), the voltages at all buses are improved.

ii) Amount of improvement in case of single feeder network is better than three feeder case because amount of power produced by the µ sources is less than the power demand by loads of the three feeder,

also the µ sources are far from loads of industrial (bus 8) and commercial (buses 9-16) feeders.

iii) The largest drop of the voltage is about 4.5% without µ sources, because we assume that the voltage at the main grid (distribution network) equal to 1 p.u., if we assume that the voltage at the distribution network less than 1 p.u (due to voltage drop in the transmission network) as actually occur, the voltage drop without using µ sources will be more than 4% and may be reach to 8%.

The total power losses for one feeder and three feeder networks at the same conditions mentioned before are evaluated and the results are shown in Figures 13 and 14.

From the above figures, the following points can be summarized:

i) The total power losses with using µ sources is less than the losses when µ sources are not used, because using µ sources reduces the distance between the load and generation and also, reduce the current flowing from the main grid. In addition, in our analysis, we calculated the losses in the transformer which connect the main grid with the micro grid network. If we take the losses in the upper distribution and transmission networks, the amount of losses will exceed the calculated value.

ii) For single feeder network, at lightly load µ sources production will feeds the load and export the remaining power to the distribution grid which make the losses with using µ sources larger than losses without µ sources.

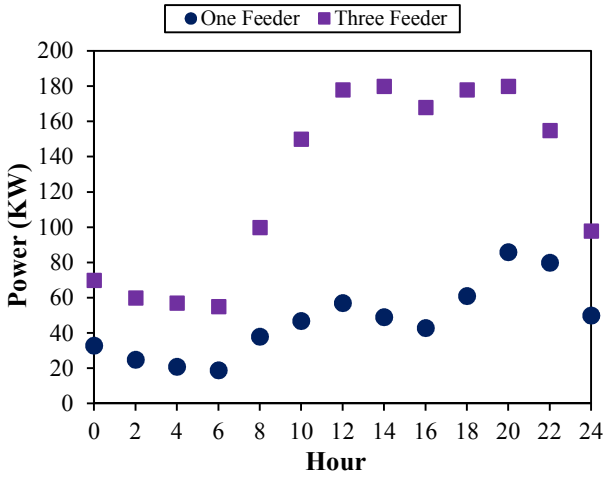

FIGURE 6: Daily load curves for one feeder and three feeders Networks.

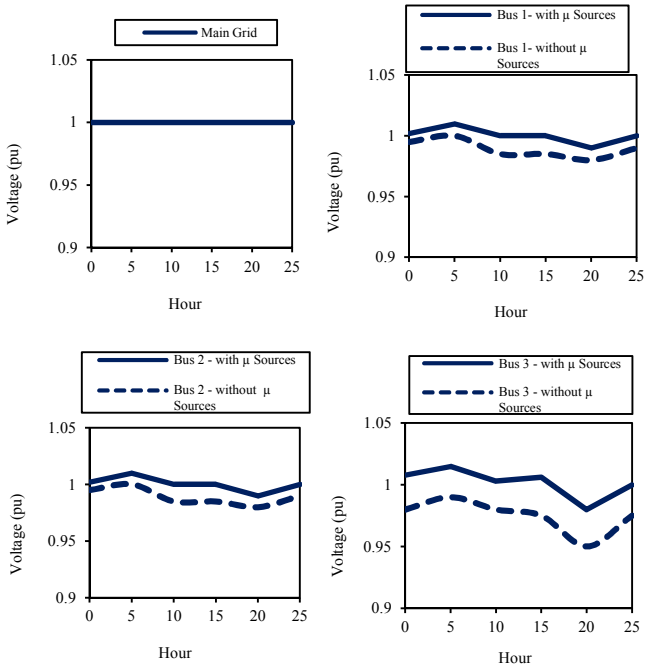

FIGURE 7: Voltage at buses 1, 2, 3 and main grid for single feeder network with and without using µ sources.

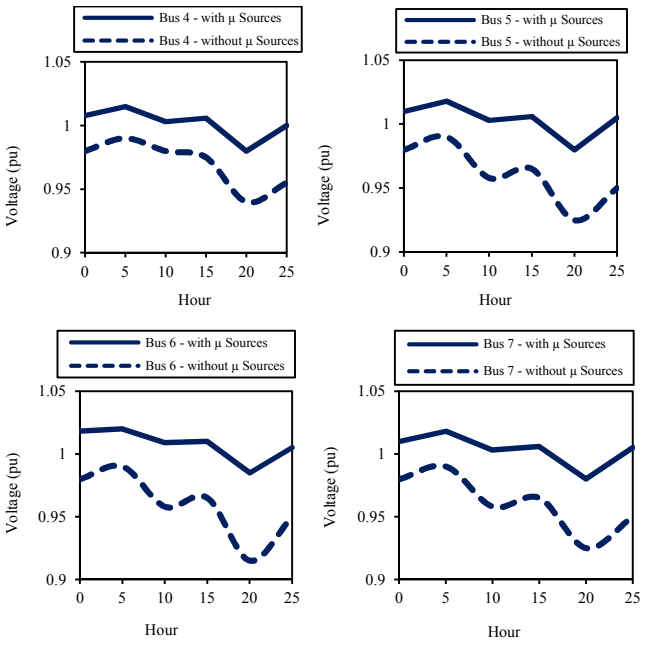

FIGURE 8: Voltage of buses 4, 5, 6 and 7 for single feeder network with and without using µ sources.

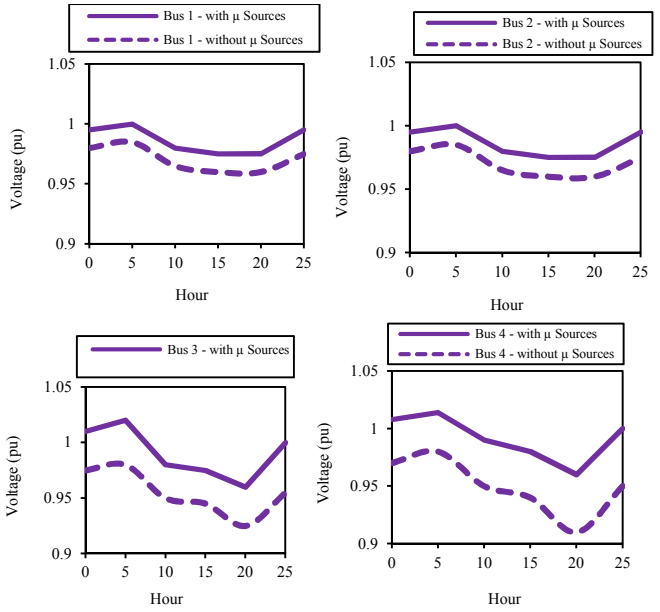

FIGURE 9: Voltage of buses 1, 2, 3 and 4 for three feeder network with and without using µ sources.

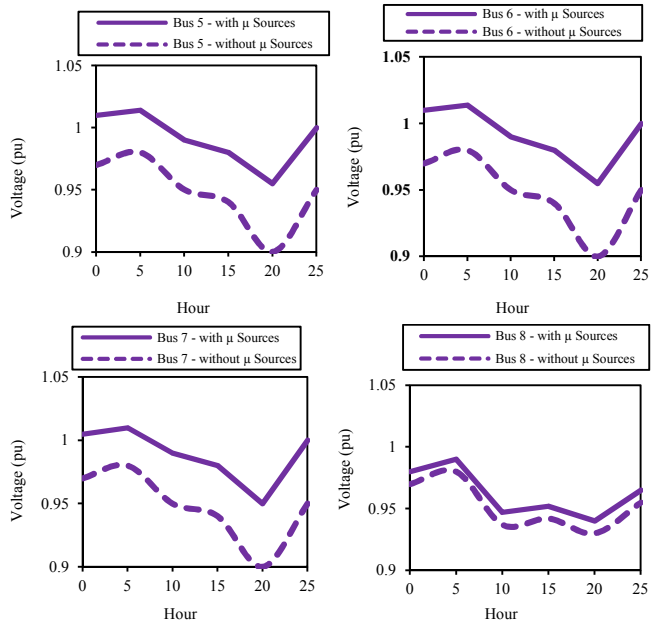

FIGURE 10: Voltage at buses 5, 6, 7 and 8 for three feeder network with and without using µ sources.

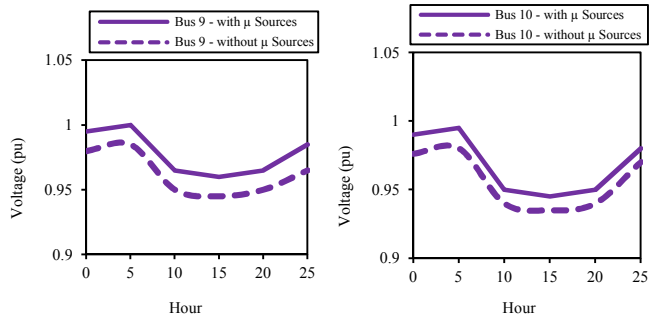

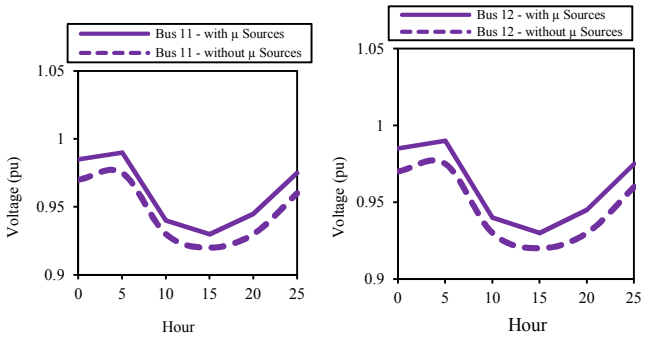

FIGURE 11: Voltage at buses 9, 10, 11 and 12 for three feeder network with and without using µ sources.

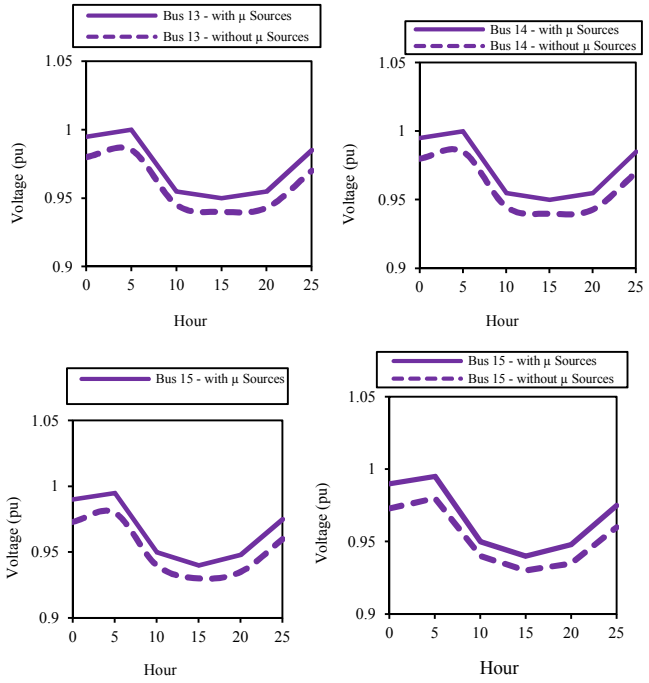

FIGURE 12: Voltage of buses 13, 14, 15 and 16 for three feeder network with and without using µ sources.

3.3. Emission Reduction Evaluation with Using µ Sources. In order to evaluate the potential of environmental benefits from the micro grids, data about the emissions from the main grid and data about the emissions of the µ sources should be taken into account. The emissions for which calculations are made are: CO_2 , SO_2, NO and particulate matters.

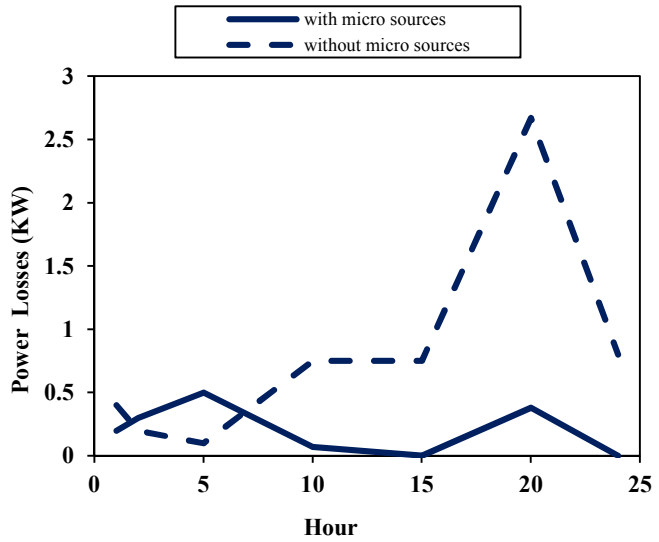

FIGURE 13: Total losses for single feeder network with and without µ sources.

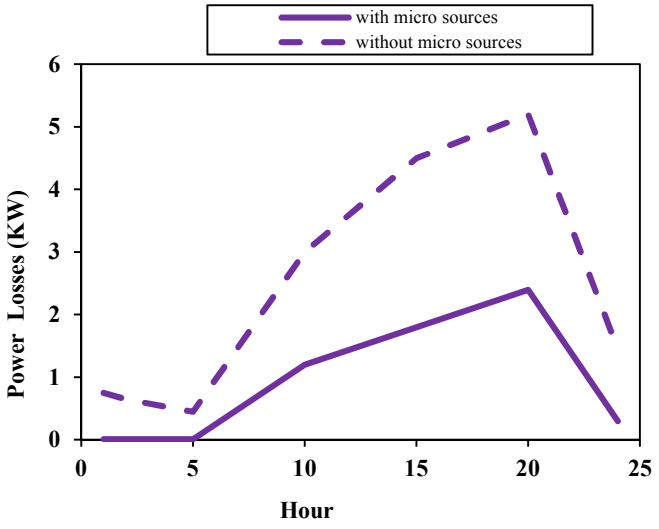

FIGURE 14: Total losses for three feeders network with and without µ sources.

3.3.1 Emissions of the Main Grid. The production of the µ sources displaces power from the main grid. Thus the emissions avoided are an average value of the main grid emissions multiplied by the production of the µ sources. In our study, typical values of emissions have been used as shown in Table 4.

TABLE 4: Typical values of emissions from the main grid.

Pollutants	Gr/ KWh
CO_2	889
SO_2	1.8
NO_x	1.6
Particulate Matters	0.501

3.3.2 Impact of µ Sources. From the installed µ sources the ones that consume fuels have emissions which are significantly lower than the ones in the main grid. Where as the renewable such as wind and solar energies have zero emissions in their operation. It is assumed that the fuel burned by the Micro turbine and the fuel cells is natural gas. Table 5 gives the data used for our analysis.

3.3.3 Results and Discussions. Amounts of emissions with and without using µ sources for single feeder and three feeder networks are shown in Figures 15 and 16. According to the results obtained in the previous figures the following point can be summarized:

i) Using µ sources has large effect in reducing the amount of emissions on CO_2, SO_2 , NOx and particulate matters, but the reduction in SO_2 , NOx and particulate matters is greater in percentage than CO_2 reduction due to the fact that the fuel burning units use natural gas that has lower emission levels in particulate matters, NOx and SO_2 compared to thermal stations that use Heavy Oil.

TABLE 5: Typical emission data for µ sources.

Unit Name	CO_2 Coeff. (gr/KWh)	NO_x Coeff. (gr/KWh)	SO_2 Coeff. (gr/KWh)	Parti. Matters (gr/KWh)
Micro turbine	724.6	0.2	0.004	0.041
Fuel Cell	489	0.01	0.003	0.001
Wind 1	0	0	0	0
PV_1	0	0	0	0
PV_2	0	0	0	0
PV_3	0	0	0	0
PV_4	0	0	0	0
PV_5	0	0	0	0

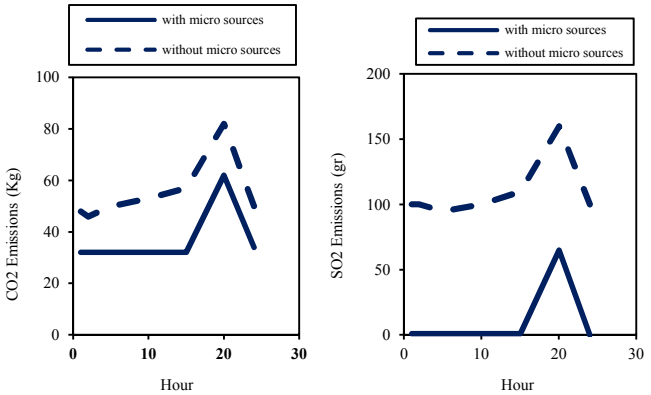

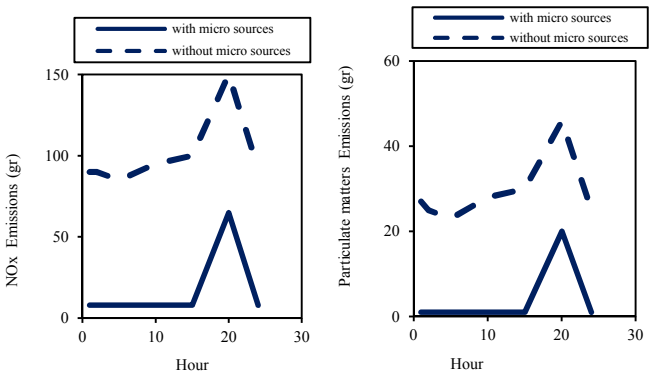

FIGURE 15: Amount of CO_2, SO_2, No_x and particulate matters emissions for one feeder network with and without µ Sources.

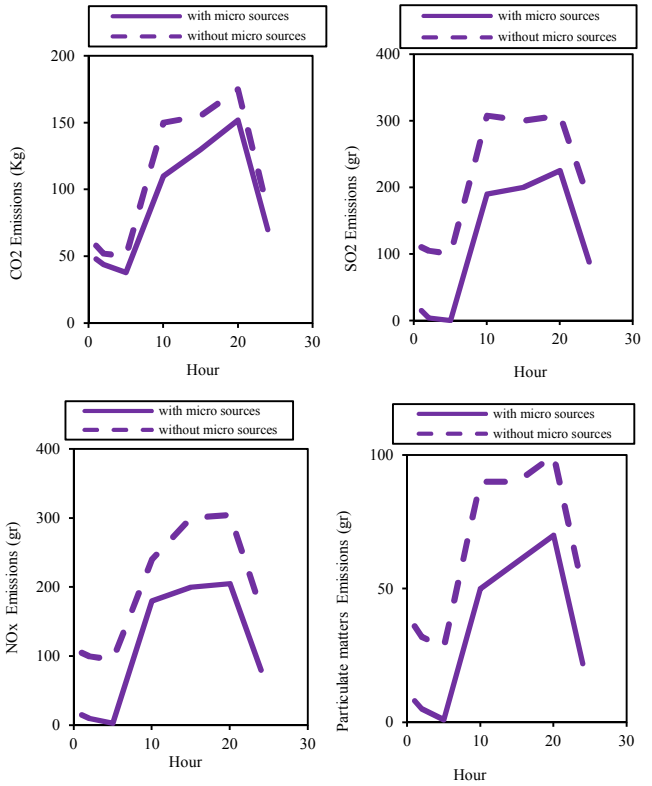

FIGURE 16: Amount of CO_2 , SO_2, NOx and particulate matters emissions for three feeder Network with and without µ sources.a

ii) In our study, the amount of power produced by renewable energy is small (15% of the µ sources power), if the renewable sources increases, amount of emissions reduction will be more than the value shown in the previous figures.

iii) The authors next step research aims to study the effects of micro grid in the dynamic performance of the main grid and how to use the µ sources to solve some of power system dynamic problems such as voltage stability, power quality and power system reliability.

4. CONCLUSIONS

The effect on convective heat transport within a closed reservoir system of varying fluid composition was analyzed by CFD modeling of a single-phase fluid with properties derived from a composition-dependent average of pure CO_2 and pure H_2O. As compositional properties were varied from H_2O toward that of CO_2, substantial increases were observed in Nusselt number (by a factor of up to 10) and normalized stream function (by a factor of up to 2.67). It is found that when the power produced by µ sources sufficient to loads, the voltage drop at all buses has a negligible values, also, using micro grid will decrease the amount of power losses because the power which produced by µ sources will consumed locally with the load near from the µ sources which prevent current from flowing or circulating in the networks transmission lines.

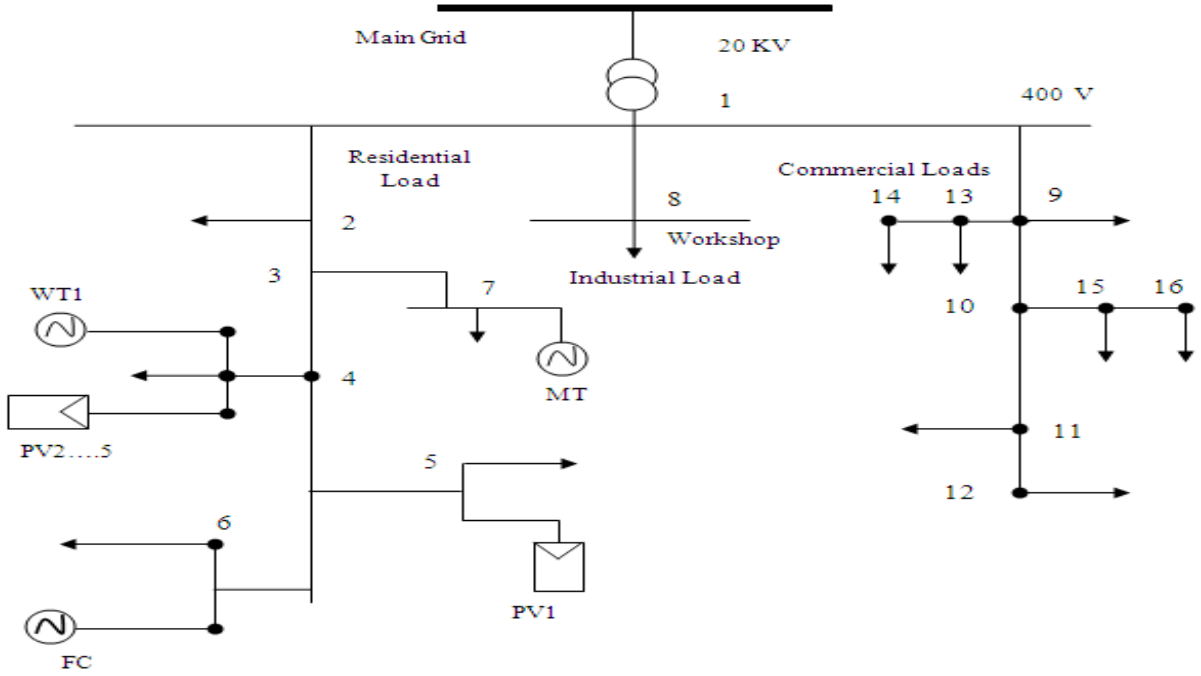

FIGURE 17: Single line diagram for three feeder network.

We conclude that this indicates substantial increase in convective heat transport. Convective heat transport may be further modified by multiphase flow behaviors, and we conclude that, due to the potential magnitude of heat flow enhancement by the addition of CO_2, further research exploring the effect of these behaviors on heat transport is warranted. These findings do demonstrate, however, that reservoirs with elevated CO_2 content will experience greater convective heat transfer and therefore be of comparatively higher temperature (and therefore of greater resource value). Additionally, it can be concluded that any increase in CO_2 content of an existing reservoir will enhance convective flow behaviors (although the true magnitude of this effect will depend on two-phase flow behavior as well as the particulars of the reservoir) and consequently will enhance the productivity and/or the longevity of geothermal energy extraction. Results also showed that using μ sources has more effects in reducing all types of emissions especially when the μ sources contains many renewable sources such as wind and solar energy sources.

CONFLICT OF INTERESTS

The authors declare that there is no conflict of interests regarding the publication of this paper.

REFERENCES

[1] A. Nago and A. Nieto, "Natural gas production from methane hydrate deposits using CO 2 clathrate sequestration: state-ofthe-art review and new technical approaches," Journal of Geological Research, vol. 2011, Article ID 239397, 6 pages, 2011.

[2] D. Pudjianto, E. Zafiropoulos and L. Daoutis, "DG4: Me- thodology for Quantifying Economic and Environmental Benefits of MicroGrids," Microgrids Project deliverable of task DG4, 2005.

[3] R. Billinton, M. Fotuhi-Firuzabad and L. bertling, "Bibliography on the Application of Probability Methods in Power System Reliability Evaluation 1996-1999," *IEEE Power Engineering Review*, Vol. 21, No. 8, 2001, p.56.

[4] P. Forooghi and K. Hooman, "Experimental analysis of heat transfer of supercritical fluids in plate heat exchangers," International Journal of Heat and Mass Transfer,vol.74,pp.448–459,2014.

[5] A. D. Atrens, H. Gurgenci, and V. Rudolph, "Water condensation in carbon-dioxide-based engineered geothermal power generation," Geothermics,vol.51,pp.397–405,2014.

[6] D. W. Brown, "A hot dry rock geothermal energy concept utilizing supercritical CO2instead of water," in Proceedings of the 25th Workshop on Geothermal Reservoir Engineering, Stanford University, Stanford, Calif, USA, 2000.

[7] K. Pruess, "Enhanced geothermal systems (EGS) using CO as working fluid—a novel approach for generating renewable energy with simultaneous sequestration of carbon," Geothermics,vol.35,no.4,pp.351–367,2006.

[8] H. Guoqiang and W. Jiong, "Extrapolation of Nystrom solution for two dimensional nonlinear Fredholm integral equations," Journal of Computational and Applied Mathematics,vol.134,no. 1-2, pp. 259–268, 2001.

[9] B. A. Goldstein, G. Hiriart, J. Tester, B. Bertani, R. Bromley, L. Gutierrez-Negrin, C. J. Huenges, E. H. Ragnarsson, A. Mongillo, M. A. Muraoka, and V. I. Zui, "Great expectations for geothermal energy to 2100," in Proceedings, ThirtySixth Workshop on Geothermal Reservoir Engineering, Stanford University, Stanford, California, 31 January–2 February, SGP-TR-191 (2011).

[10] C. Augustine, K. R. Young, and A. Anderson, "Updated U.S. geothermal supply curve," in Proceedings, Thirty-Fifth Workshop on Geothermal Reservoir Engineering, Stanford University, Stanford, California, 1 February–3 February, 2010, SGP-TR-191 (2010).

[11] F. Kanyako and I. Janajreh, "Vertical axis wind turbine performance prediction for low wind speed environment," in 2014 IEEE Innovations in Technology Conference (InnoTek) (2014), pp. 1–10.

[12] D. B. Fox, D. Sutter, K. F. Beckers, M. Z. Lukawski, D. L. Koch, B. J. Anderson, and J. W. Tester, "Sustainable heat farming: Modeling extraction and recovery in discretely fractured geothermal reservoirs," Geothermics 46, 42–54 (2013).

[13] J. W. Lund, "Direct utilization of geothermal energy," Energies 3(8), 1443–1471 (2010).

[14] D. Pudjianto, E. Zafiropoulos and L. Daoutis, "DG4: Me- thodology for Quantifying Economic and Environmental Benefits of MicroGrids," Microgrids Project deliverable of task DG4, 2005.

[15] Anvari Moghaddam, A. ; Seifi, A.R. (2010b). Improvement of Power Systems Operation Using Smart Grid Technology. *First Iranian Conference on Renewable Energies and Distributed Generation (ICREDG'10)*, March 9-11, 2010, Birjand, Iran.

[16] F. A. Al-Sulaiman, F. Hamdullahpur and I. Dincer, "Trigeneration: A Comprehensive Review Based on Prime Movers," *International Journal of Energy Research*, Vol. 35, No. 3, 2010, pp.233-258.doi:10.1002/er.1687.

[17] H. Ghaebi, M. Amidpour, S. Karimkashi and O. Rezayan, "Energy, Exergy and Thermoeconomic Analysis of a Combined Cooling, Heating and Power (CCHP) System with Gas Turbine Prime Mover," *International Journal of Energy Research*, Vol. 35, No. 8, 2010, pp. 697-709. doi:10.1002/er.1721.

[18] E. Cardona, A. Piacentino and F. Cardona, "Matching Economical, Energetic and Environmental Benefits: An Analysis for Hybrid CHCP-Heat Pump Systems," *Energy Conversion and Management*, Vol. 47, No. 20, 2006, pp. 3530-3542. doi:10.1016/j.enconman.2006.02.027.

[19] A. K. Hueffed and P. J. Mago, "Influence of Prime Mover Size and Operational Strategy on the Performance of Com- bined Cooling, Heating, and Power Systems under Diffe- rent Cost Structures," *Journal of Power and Energy*, Vol.224, No. 5, 2010, pp. 591-605.

[20] *Energy Statistics Handbook—2010* [in Chinese]; Bureau of Energy (BOE): Taipei, Taiwan, 2011.

[21] *Statistics on Emissions of CO from Combustion and Its Analysis* [in Chinese]; Bureau of Energy (BOE): Taipei, Taiwan, 2011.

[22] Huang, Y.H.; Wu, J.H. Energy policy in Taiwan: Historical developments, current status and potential improvements. *Energies* 2009, *2*, 623–645.

[23] Tsai, W.T.; Hsien, K.J. An analysis of cogeneration system utilized as sustainable energy in the industrial sector in Taiwan. *Renew. Sustain. Energy Rev.* 2007, *11*, 2104–2120.